Bulletin of the Seismological Society of America, Vol. 97, No. 5, pp. 1486–1501, October 2007, doi: 10.1785/0120060255

Quantitative Classification of Near-Fault Ground Motions Using Wavelet Analysis

by Jack W. Baker

Abstract A method is described for quantitatively identifying ground motions containing strong velocity pulses, such as those caused by near-fault directivity. The approach uses wavelet analysis to extract the largest velocity pulse from a given ground motion. The size of the extracted pulse relative to the original ground motion is used to develop a quantitative criterion for classifying a ground motion as "pulse-like." The criterion is calibrated by using a training data set of manually classified ground motions. To identify the subset of these pulselike records of greatest engineering interest, two additional criteria are applied: the pulse arrives early in the ground motion and the absolute amplitude of the velocity pulse is large. The period of the velocity pulse (a quantity of interest to engineers) is easily determined as part of the procedure, using the pseudoperiods of the basis wavelets. This classification approach is useful for a variety of seismology and engineering topics where pulselike ground motions are of interest, such as probabilistic seismic hazard analysis, ground-motion prediction ("attenuation") models, and nonlinear dynamic analysis of structures. The Next Generation Attenuation (NGA) project ground motion library was processed using this approach, and 91 large-velocity pulses were found in the fault-normal components of the approximately 3500 strong ground motion recordings considered. It is believed that many of the identified pulses are caused by near-fault directivity effects. The procedure can be used as a stand-alone classification criterion or as a filter to identify ground motions deserving more careful study.

Introduction

Near-fault ground motions containing strong velocity pulses are of interest in the fields of seismology and earthquake engineering. A quantitative approach for identifying these ground motions is proposed here and used to perform a variety of basic studies of their properties. These ground motions, which are here referred to as "pulselike ground motions," have been identified as imposing extreme demands on structures to an extent not predicted by typical measures such as response spectra (e.g., Bertero *et al.*, 1978; Anderson and Bertero, 1987; Hall *et al.*, 1995; Iwan, 1997; Alavi and Krawinkler, 2001; Menun and Fu, 2002; Makris and Black, 2003; Mavroeidis *et al.*, 2004; Akkar *et al.*, 2005; Luco and Cornell, 2007). Theoretical considerations also provide an indication of seismological conditions that may result in occurrence of velocity pulses due to, for example, directivity effects (Somerville *et al.*, 1997; Somerville, 2003; Spudich *et al.*, 2004). While the effect is relatively well studied, a hindrance to incorporating these effects in probabilistic seismic hazard analysis and engineering building codes is that a quantitative method for identifying these velocity pulses does not yet exist. This means that a variety of researchers have assembled sets of pulselike or near-fault ground motions, but these classifications are not easily reproducible (e.g., Mavroeidis and Papageorgiou, 2003; Somerville, 2003; Fu and Menun, 2004; Akkar *et al.*, 2005).

The ground motions identified in past studies are typically selected because the velocity time history of the ground motion is dominated by a large pulse, as seen, for example, in Figure 1a, and/or because source–site geometry suggests that a directivity pulse might be likely to occur at the site where the motion was recorded. Selection of pulselike ground motions using these approaches requires some level of judgment, and for many ground motions, such as those shown in Figure 1b and c, the classification may not be obvious. Identification of non-pulselike motions at near-fault locations (such as the one shown in Fig. 1d) is also challenging for the same reasons, although it has not received as much attention.

The lack of a quantitative classification scheme for recorded ground motions has hindered progress toward obtaining results such as the probability that a ground motion with a given earthquake magnitude, distance, and source–site geometry will contain a velocity pulse. Knowledge of this probability is useful for applications such as probabilis-

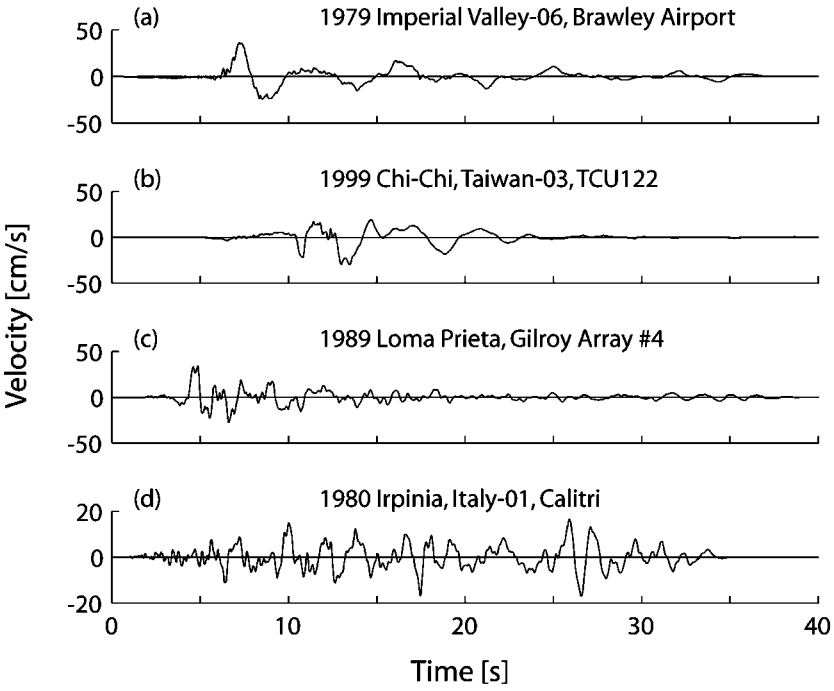

Figure 1. Example fault-normal near-fault ground motions. (The pulse indicator values for these four ground motions, from top to bottom, are 1.00, 0.39, 0.27, and 0.00.)

tic seismic hazard analysis (I. Iervolino and C. A. Cornell, unpublished manuscript, 2007; Tothong *et al.*, 2007). The lack of quantitative classifications also means that electronic libraries of recorded ground motions do not list any statistics indicating whether a given ground motion contains a velocity pulse, and this limits the ability of the science and engineering communities to access these ground motions and study their effects for research or practical applications.

In this article, an approach for detecting pulses in ground motions is proposed and investigated. The procedure uses wavelet-based signal processing to identify and extract the largest velocity pulse from a ground motion; if the extracted pulse is "large" relative to the remaining features in the ground motion, the ground motion is classified as pulselike. The period of a detected velocity pulse, a parameter of interest to engineers, is also easily determined. The classification algorithm is computationally inexpensive, so large libraries of recorded ground motions can be (and have been) analyzed. Although some of the identified pulses are likely not caused by directivity effects, the approach is useful for identifying a set of records potentially exhibiting directivity effects, which can then be manually considered more carefully. Alternatively, the ground motions could be used (without further classification) for structural response calculations, under the assumption that pulses will cause similar effects regardless of their causal mechanism.

Causes of Velocity Pulses

For the purposes of this study, a pulselike ground motion is considered to be a record with a short-duration pulse that occurs early in the velocity time history and has large amplitude (as defined precisely subsequently). One cause of these velocity pulses is forward-directivity effects in the near-fault region. Forward directivity results when the fault rupture propagates toward the site at a velocity nearly equal to the propagation velocity of the shear waves and the direction of fault slip is aligned with the site. This causes the wavefront to arrive as a single large pulse. A more detailed description of this phenomenon is given by, for example, Somerville *et al.* (1997). For both strike-slip and dip-slip faults, forward directivity typically occurs in the fault-normal direction. For this reason, results from the fault-normal components of ground motions are emphasized here. Another near-fault effect, fling step, is mentioned for completeness but not considered in depth here. This permanent displacement of the ground resulting from fault rupture, in general, is not detected by the procedure because the residual displacements are not detected by the pulse model used in the following text.

Directivity effects are a major concern for researchers studying velocity pulses, and many of the pulses identified in the following text were likely caused by directivity effects (as judged by considering their source–site geometry). Other phenomena, however, may also cause velocity pulses. If a site is located near an asperity in the fault rupture, the waves caused by that asperity may produce a pulse at the site. Constructive interference of seismic waves passing through a complicated earth structure such as the edge of a geologic basin might also result in velocity pulses. Although directivity effects are the presumed cause of many near-fault pulses, the signal-processing approach described here is not able to distinguish between the potential causal mechanisms. More careful analysis would be needed to incorporate knowledge of the site location and the fault geometry and slip.

Choice of a Classification Procedure

When selecting a classification procedure, several criteria were deemed to be important. Most critically, the procedure should be able to distinguish between a pulse and a nonpulse. As will be seen subsequently, this distinction is not intrinsically binary, but it is straightforward to rank the records and determine some threshold at which to make a binary classification. The classification procedure should require minimal intervention or judgment from the analyst and should produce a consistent and reproducible result, so that classifications of a given ground motion are consistent from analyst to analyst. A computationally inexpensive procedure is also preferable, because thousands of recorded ground motions will be processed.

These goals are best met by using a relatively simple pulse classification. Others have developed detailed models to describe the shape of velocity pulses (Mavroeidis and Papageorgiou, 2003; Fu and Menun, 2004). Those models are very useful for other applications but here a simple classification is more useful for automated screening and classification of large numbers of ground motions. An analogy with soil-type classifications may be useful: local soil geology can be quite complex and so detailed models are sometimes developed, but for practical applications simplified classifications are often used (e.g., several common criteria classify all site conditions into four or five groups).

A type of signal processing known as wavelet analysis is well suited for this classification task. It is computationally inexpensive and outputs quantitative and reproducible results. Velocity pulses can be easily identified and extracted, and these extracted pulses can be used both for classification and for other parametric studies.

Wavelet Analysis

Wavelet analysis has undergone rapid theoretical and application-oriented development in the past 20 years, as its usefulness for a range of problems has been explored. There is a wide literature available regarding theoretical features of the approach as well as algorithmic details (e.g., Mallat, 1999), so only a brief overview of the most relevant features is provided here. A basic understanding can be gained through comparison with Fourier analysis. Fourier analysis represents a signal using a linear combination of sine waves, each representing a signal of infinite length and a single frequency. In contrast, wavelet analysis decomposes a signal into wavelets that are localized in time and that represent a narrow range of frequencies. For nonstationary signals such as earthquake ground motions, it can be advantageous to represent the signal as a summation of wavelets rather than a summation of stationary sine waves.

Wavelets are basis functions that satisfy a certain set of mathematical requirements. Many wavelet prototypes can be used to decompose a signal (see Fig. 2 for examples). The prototype function is referred to as a mother wavelet, and this function is scaled and translated in time to form a set of basis functions. A variety of theoretical considerations regarding the choice of a useful mother wavelet function include: orthogonality, compactness, number of derivatives, symmetry, etc. (Mallat, 1999). The wavelets shown in Figure 2 are all widely used and suitable for application here.

The wavelet basis function at time t is defined mathematically by

$$\Phi_{s,l}(t) = \frac{1}{\sqrt{s}} \Phi \left(\frac{t - l}{s} \right), \quad (1)$$

where $\Phi(\cdot)$ is the mother wavelet function, s is the scale parameter that dilates the wavelet, and l is the location parameter that that translates the wavelet in time. Any signal $f(t)$ can be represented as a linear combination of basis functions, and the coefficients for that linear combination are determined by the following convolution integral, which is identical in concept with the Fourier transform calculation. The coefficient associated with the wavelet having scale s and position l is given by

$$C_{s,l} = \int_{-\infty}^{\infty} f(t)\Phi_{s,l}(t)\, dt = \int_{-\infty}^{\infty} f(t) \frac{1}{\sqrt{s}} \Phi \left(\frac{t - l}{s} \right) dt. \quad (2)$$

To analyze digital signals such as the ground-motion velocity time histories considered here, equation (2) is discretized into a summation rather than an integral, but the principle remains the same.

There are two classes of wavelet transforms used to analyze a signal, depending on the number of scales and locations for which coefficients are computed. The continuous wavelet transform computes the wavelet coefficients associated with every integer value of the scale and location parameters. This provides detailed information about the time–frequency characteristics of the signal. But a digital signal of length n can be fully described using a reduced number of coefficients. If the wavelets are orthogonal, then only n wavelets are needed to completely describe any discrete time signal of length n. The discrete wavelet transform provides the n coefficients describing the amplitude of the n wavelets at various scales and locations. If n is a power of 2, then an extremely efficient algorithm exists to perform the calculations (analogous to the fast Fourier transform). Coefficients from continuous and discrete wavelet transforms of an example ground motion are shown in Figure 3 to illustrate the difference between these two approaches.

Further, if the mother wavelet closely represents the shape of the features of interest, then even fewer than n coefficients are needed to closely represent the signal. A few coefficients will be large and their associated wavelets will represent major features of the signal. Many other coefficients will be close to zero because the associated wavelet represents relatively small features. This phenomenon forms the basis of many signal denoising and data compression

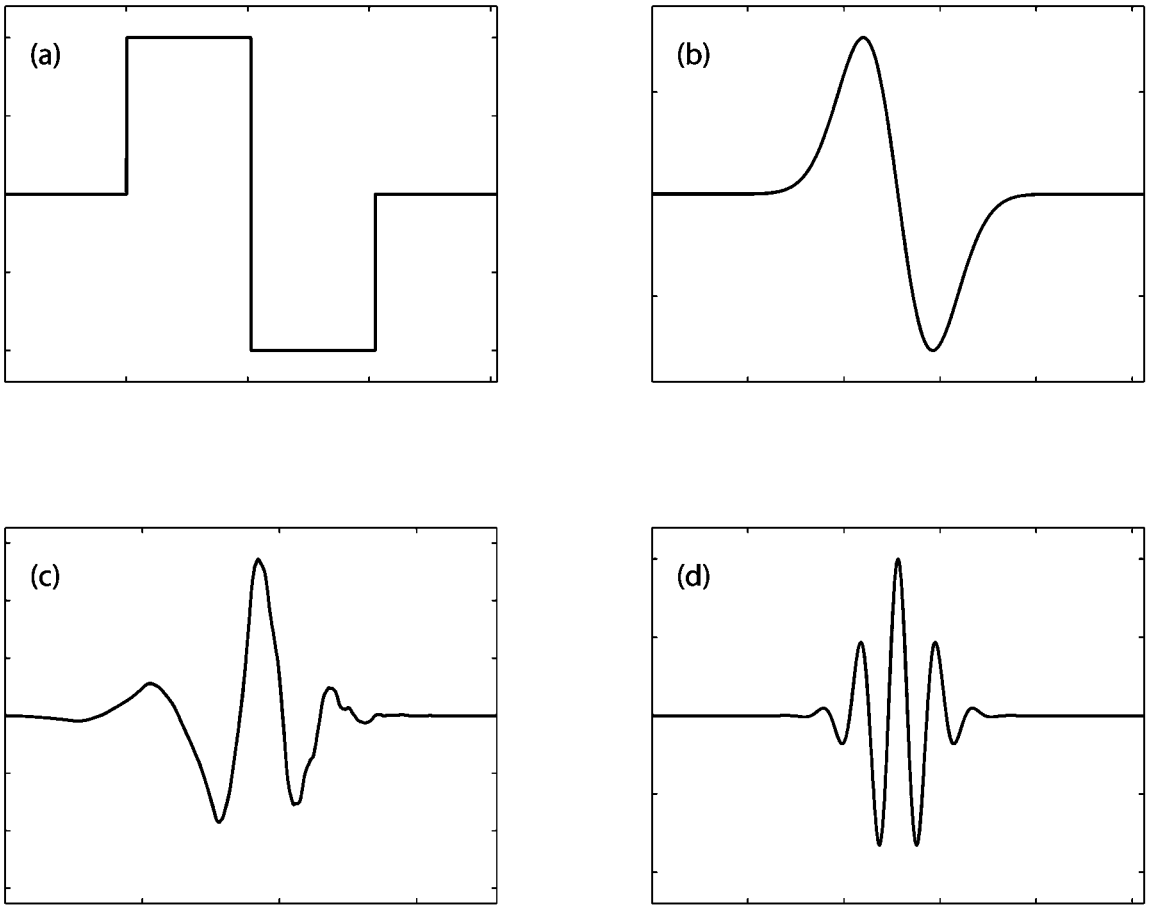

Figure 2. Common mother wavelets used for wavelet analysis: (a) Haar wavelet, (b) Gaussian wavelet of order 1, (c) Daubechies wavelet of order 4, and (d) Morlet wavelet.

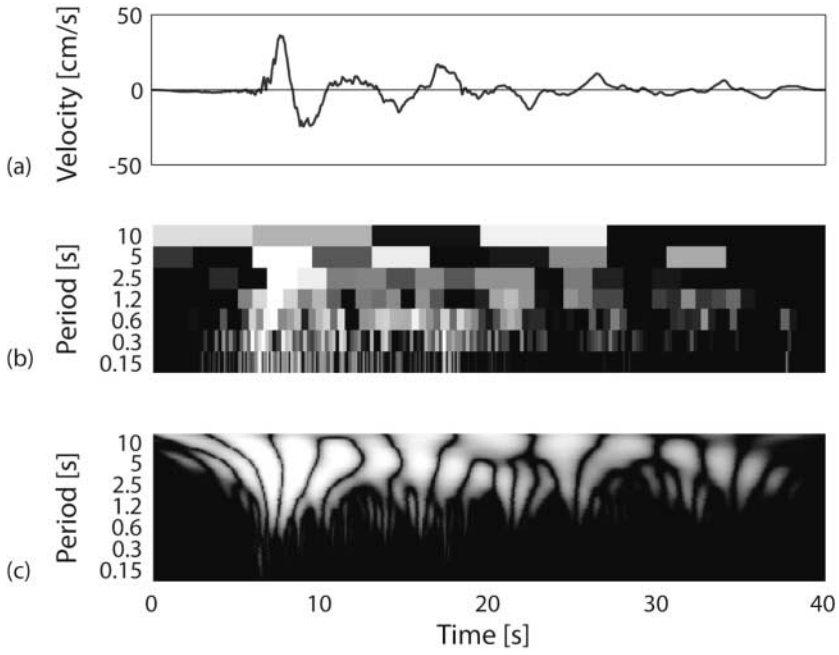

Figure 3. (a) Example ground-motion velocity time history (the fault-normal component of the 1979 Imperial Valley, Brawley Airport recording). (b) Discrete wavelet transform coefficients. (c) Continuous wavelet transform coefficients. In plots (b) and (c), light shading indicates a large absolute value of the coefficient with the specified period and location in time.

applications. Here it will be used for a different purpose: if a significant portion of a ground-motion time history is described by one or a few wavelets with large coefficients, then this will be used to indicate the presence of a pulse.

Both the continuous and discrete wavelet transforms have features that make them potentially useful for this application. Whereas the continuous transform has greater computational expense and produces many more coefficients than are needed to describe the signal, its higher resolution is useful for precisely identifying the largest coefficient, which will here indicate the period and location of the near-fault pulse. Further, unlike the discrete wavelet transform, the coefficients obtained from the continuous wavelet transform do not change if the beginning or end of the signal is padded with additional zeros. This is helpful because it is undesirable to work with coefficients that depend on irrelevant features such as when the ground-motion instrument started and stopped recording. For these reasons, the continuous wavelet transform is used in the classification criterion described next.

Classification of Signals

The procedure described in this section utilizes wavelet analysis to identify near-fault ground motions containing velocity pulses. The largest pulse in the ground motion is extracted to determine whether it represents a significant portion of the signal. Two additional optional criteria are also useful for identifying those pulselike ground motions most likely to be caused by directivity effects; checks are performed to verify that the identified pulse arrives early in the ground motion (indicating that it is likely due to directivity effects) and that the ground motion has a high peak velocity (to eliminate, for example, ground motions from small earthquakes that might appear pulselike only because the time history is simple).

Extraction of the Velocity Pulse

For each ground motion under consideration, the largest velocity pulse was extracted using the wavelet decomposition described briefly previously. The Daubechies wavelet of order 4, shown in Figure 2c, is used as the mother wavelet here because it approximates the shape of many velocity pulses and it was seen to perform well relative to the other candidate mother wavelets. To evaluate a ground motion, first the continuous wavelet transform of the velocity time history is computed, and the coefficient with the largest absolute value is identified. The wavelet associated with this coefficient identifies the period and location of the pulse, as illustrated in Figure 4a. (Note that a wavelet coefficient is equal to the energy of the associated wavelet, so the selected pulse is also the one with the largest energy.) This wavelet is subtracted from the ground motion, and the continuous wavelet transform is computed for the residual ground motion. Because the location and period of the pulse have been identified, only wavelets having the same period and located at nearby times (within $\pm$ one-half of the width of the original wavelet signal, s) are considered at this step. The largest of these coefficients is identified, as illustrated in Figure 4b. Often only one or two coefficients are needed to describe the pulse, but a total of ten coefficients in the identified period and location window are extracted in the algorithm to ensure that the pulse is represented in a detailed manner. An extracted pulse using ten coefficients is illustrated in Figure 4c, and the residual ground motion after the pulse has been removed is shown in Figure 4d. An example of the acceleration, velocity, and displacement time histories associated with an extracted pulse are shown in Figure 5. The extracted pulse clearly captures the velocity and displacement pulses, while ignoring the high-frequency motion that dominates the acceleration time history of the original ground motion. As mentioned earlier, the wavelet basis functions used for this extraction have by definition zero residual displacement, so fling effects will not be detected.

By using this procedure, a pulse can be extracted from any ground motion, whether a significant directivity pulse exists or not. For non-pulselike records, however, the extracted pulse is typically a minor feature of the ground motion and the residual ground motion is nearly identical with the original motion. To classify the records, it is thus necessary to identify properties of the extracted pulses that can be used for automated classification.

Determination of the Significance of the Extracted Pulse

The original ground motions and residuals after pulse extraction can be used to predict whether the given ground motion is pulselike. To perform this classification, a variety of potential predictor variables were computed and evaluated to determine whether they were useful indicators of the presence of a pulse. A difficulty arises, however, because there is no existing classification of a large dataset to use for calibrating the prediction algorithm. The challenges relating to classifications were discussed in the introduction and illustrated in Figure 1.

The approach used here is to first manually classify a set of records and then build a statistical predictive model that is able to closely reproduce the classifications of this training data. To build a training set of classifications, all fault-normal ground motions in the Next Generation Attenuation (NGA) ground motion library (http://peer.berkeley.edu/nga) with magnitudes greater than 5.5 and recorded within 30 km of an event were selected (note that the records available online were rotated to fault-normal orientations). The 398 selected records were then manually classified by the author based on visual inspections to identify pulses in their velocity time histories. Records with obvious pulselike or non-pulselike characteristics, such as the records in Figure 1a and d, were classified appropriately. Records with no clear classification, such as those in Figure 1b and c, were

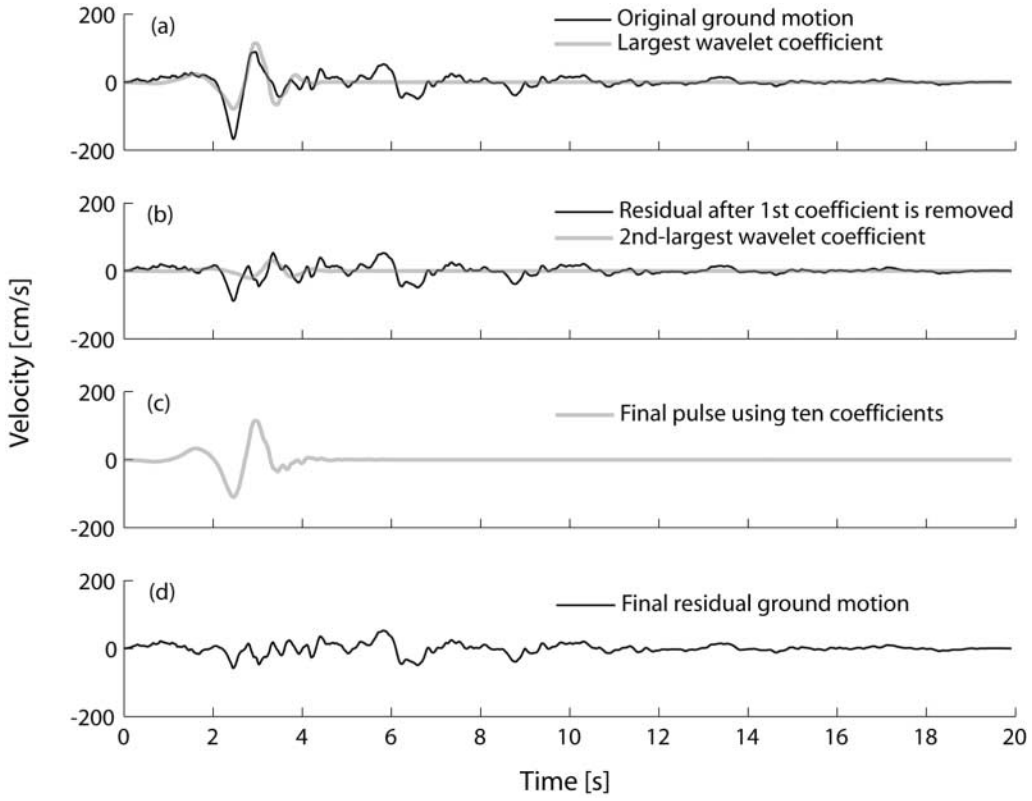

Figure 4. Illustration of the decomposition procedure used to extract the pulse portion of a ground motion (the fault-normal component of the 1994 Northridge, Rinaldi, recording).

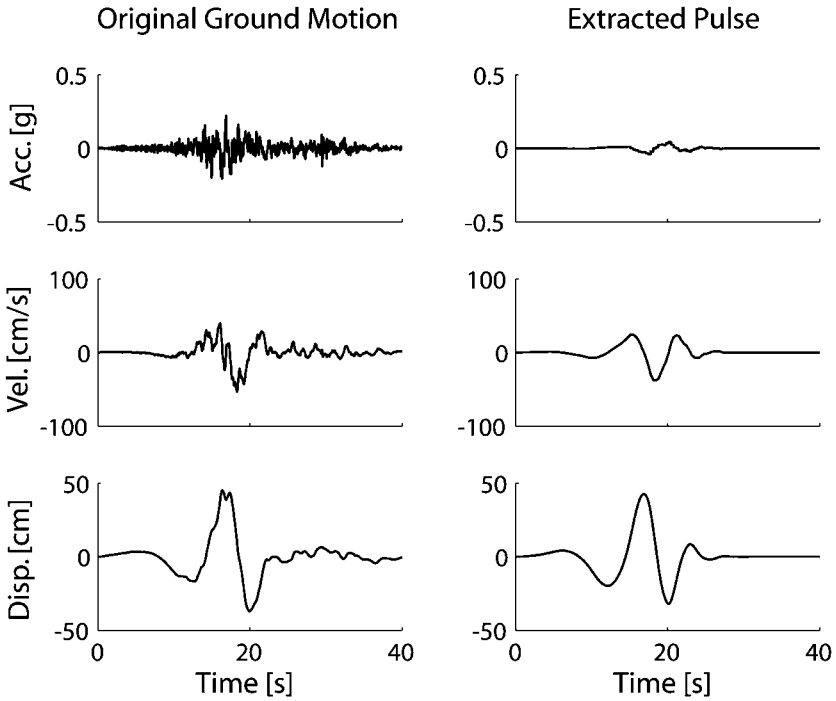

Figure 5. Acceleration, velocity, and displacement time histories of the 1992 Landers, Yermo Fire Station, ground motion, and the extracted pulse associated with this ground motion.

classified as ambiguous and treated separately when evaluating the effectiveness of wavelet criteria. The classifications were performed using only visual inspections of the velocity time histories; no additional seismological information was used, and no attempt was made at this stage to eliminate late-arriving pulses or simple low-amplitude ground motions that look pulselike. This manual classification produced 124 potentially pulselike ground motions, 190 non-pulselike ground motions, and 84 ambiguous ground motions. Once manual classifications of these ground motions were determined, statistical prediction tools were used to reproduce the manual classifications based on automated predictions using outputs from the wavelet analysis.

Linear discriminant analysis was used to evaluate the ability of potential predictors to distinguish between pulselike motions having large extracted pulses and non-pulselike ground motions having insignificant extracted pulses. A variety of predictor variables were considered, including the size of coefficients obtained from the wavelet decomposition, response spectral values, peak ground velocities, and energy-based values. Sets of one, two, and three predictors were used simultaneously to replicate the manual classifications of the records. Two predictor variables were identified that were easy to compute, were intuitive, and provided good predictive ability: the peak ground velocity (PGV) of the residual record divided by the original record's PGV, and the energy of the residual record divided by the original record's energy (where energy can be computed as the cumulative squared velocity of the signal, or, equivalently, as the sum of the squared discrete wavelet coefficients). These variables will be referred to as the "PGV ratio" and the "energy ratio." A scatter plot of the PGV ratio versus energy ratio for the manually classified records is shown in Figure 6, indicating that the classifications can be reasonably reproduced using these two predictor variables.

Logistic regression was then used to classify the records based on these two predictors to compute their accuracy (Agresti, 2002). The logistic regression provides the following predictive equation:

$$\text{Pulse indicator} = \frac{1}{1 + e^{-23.3 + 14.6(\text{PGV ratio}) + 20.5(\text{energy ratio})}}, \quad (3)$$

where pulse indicator is a predictor of the likelihood that a given record is pulselike, based on the fraction of records with the same characteristics that were manually classified as pulselike. Pulse indicator takes values between 0 and 1, with high values providing a strong indication that the ground motion is pulselike. The predictions are continuous, which raises the question of how to use them if a discrete classification is desired. Here, records with scores above 0.85 and below 0.15 are classified as pulses and nonpulses, respectively, based on inspection of the results shown in Figure 6. The ranges of PGV ratio and energy ratio corresponding to these classifications are labeled in Figure 6. Note that the ground motions manually classified as ambiguous are omitted from Figure 6 for clarity, but they mostly fall in the region labeled as ambiguous.

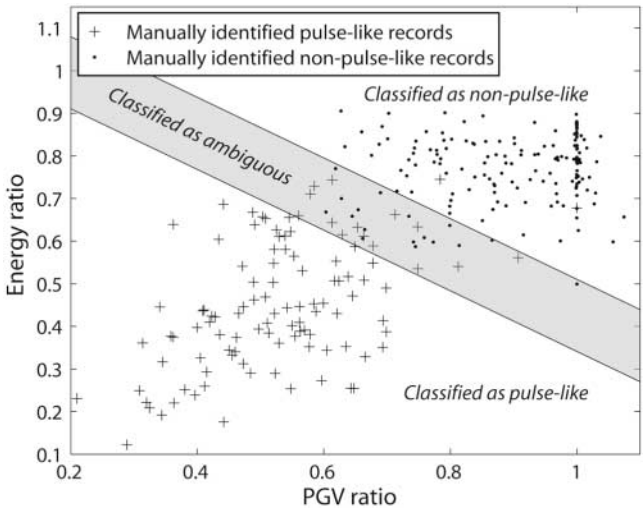

Figure 6. Scatter plot of the predictor variables used for classification. The ground motions used for training are plotted with markers indicating their classification, and the regions corresponding to each manual classification category are labeled.

Of the ground motions manually classified as pulselike or non-pulselike, 88% were classified in the same manner by the automated procedure, 11% were classified as ambiguous, and 1% were misclassified. When the records whose classifications were not reproduced were examined more closely, the automatic classifications were generally found to be reasonable. The classification algorithm actually identified three ground motions whose initial manual classifications were clearly incorrect due to human error by the author (which to some extent is inevitable when hundreds of records are being studied). The 1% of misclassified records consist of two records whose pulses were not detected by the automatic pulse extraction scheme (i.e., the pulse extracted because it had the largest energy differed in frequency or location from the pulse an analyst would identify visually). While the pulse extraction criterion could be modified so that the two missed pulses are detected, the conceptual simplicity of the proposed approach (which selects the pulse having the largest energy) is appealing to an extent that modifying the approach to address a 1% misclassification rate did not seem reasonable. Further, the manual classifications of the two misclassified ground motions were debatable. Thus, although the manual classifications were useful for initially calibrating the procedure, the automatic classification approach may be at least as accurate and is certainly more convenient and reproducible.

Although the continuous pulse indicator values of equation (3) were used here to produce binary ground-motion classification, this discretization may not be necessary in all

situations. For example, one can use the pulse indicator to rank ground motions according to their "pulsivity" and to study the relationship between the pulse indicator and structural response. One could also use only the ground motions with the largest pulse indicator values if only a few strongly pulselike ground motions are needed for a given application.

Exclusion of Late-Arriving Pulses

Although the ground motions classified as pulselike in the previous section all have significant pulselike features, these features are likely caused by a variety of effects. If directivity effects are of primary interest, an additional criterion would be useful for identifying pulses arriving early in the velocity time history, where theoretical seismology predicts that directivity pulses will occur.

Late-arriving pulses can be identified by computing the cumulative squared velocity of both the original record and the extracted pulse. At time t, the cumulative squared velocity (CSV) would be computed as

$$\mathrm{CSV}(t) = \int_0^t V^2(u)\, du, \tag{4}$$

where CSV(t) denotes the cumulative squared velocity at time t and $V(u)$ is the ground-motion velocity at time u. By evaluating this CSV(t) function for the original ground motion and extracted pulse, the times at which each reaches $x\%$ of its total CSV are determined. These times are denoted $t_{x\%,\mathrm{orig}}$ and $t_{x\%,\mathrm{pulse}}$, for the original ground motion and extracted pulse, respectively.

By adjusting the percentage criteria for the two ground motions, it was determined that early-arriving pulses have $t_{20\%,\mathrm{orig}}$ values that are greater than $t_{10\%,\mathrm{pulse}}$ (i.e., for the extracted pulse to be at the beginning of the ground motion, it should reach 10% of its total CSV before the original ground motion reaches 20% of its CSV). Loosely, this ensures that the pulse starts before a significant portion of the original ground motion's CSV is observed. Examples an early-arriving and a late-arriving pulse are shown in Figures 7 and 8, respectively. Whereas late-arriving pulses can be excluded in an effort to identify only ground motions with directivity effects, some applications may not require this criterion. Future research is planned to study the question of whether late-arriving pulses affect structures in the same manner as early-arriving pulses.

Exclusion of Ground Motions with PGV $<$ 30 cm/sec

A final situation considered here is that some relatively low-intensity ground motions appear pulselike merely because the velocity time history is simple. This is observed in some low-magnitude events that have a small source area and consequent brief duration of the far-field *S*-wave pulse. For example, the ground motion shown in Figure 9 came from a magnitude 5.1 earthquake. Although the apparent pulselike feature may or may not be caused by directivity effects, in general, it is of no interest in engineering practice because it does not have the potential to damage structures.

To exclude these low-amplitude records, ground motions with PGVs less than some threshold can be excluded. Several threshold levels of PGV were considered, and a 30 cm/sec level was seen to eliminate nearly all small-magnitude and large-distance ground motions, while retaining the damaging pulselike ground motions (which are also more likely to be caused by directivity effects).

The three criteria described earlier can be combined in various manners to select some subset of pulselike ground motions. To provide example results, all fault-normal ground motions from the NGA ground-motion library were analyzed, and 91 were found to meet all three of the potential criteria:

1. The pulse indicator value, as defined in equation (3), is greater than 0.85.
2. The pulse arrives early in the time history, as indicated by $t_{20\%,\mathrm{orig}}$ values that are greater than $t_{10\%,\mathrm{pulse}}$.
3. The original ground motion has a PGV of greater than 30 cm/sec.

The ground motions satisfying all three criteria are listed in Table 1.

Although these three criteria identify ground motions of engineering interest because of their large amplitude and potential directivity effects, ground motions satisfying less than three may also be of interest. The cause of the late-arriving pulses (i.e., those satisfying criterion 1, but not satisfying criterion 2) has yet to be determined. Those late-arriving pulses may be of interest to engineers interested in the effects of pulses in ground motions but may not be of interest to researchers trying to empirically identify the circumstances under which directivity pulses are observed. Alternatively, one could add additional criteria (based on, e.g., source–site geometry or source inversions) to further ensure that the identified pulses are due to directivity effects. Thus, the preceding criteria might be modified depending on the specific goals of individual scientists and engineers, but the tools described here should provide a useful foundation for a range of further research activities.

Identification of Pulse Period

The period of the velocity pulse is an important parameter for structural engineers, as the ratio of the pulse period to the fundamental period of the structure can greatly affect the structure's response (Anderson and Bertero, 1987; Alavi and Krawinkler, 2001; Mavroeidis *et al.*, 2004). By examining the dominant frequency of the wavelet used to identify a ground motion's velocity pulse, it is straightforward to compute a pulse period as part of this analysis.

No well-defined concept of periods exists for wavelets such as there is for sine waves in Fourier analysis, but the

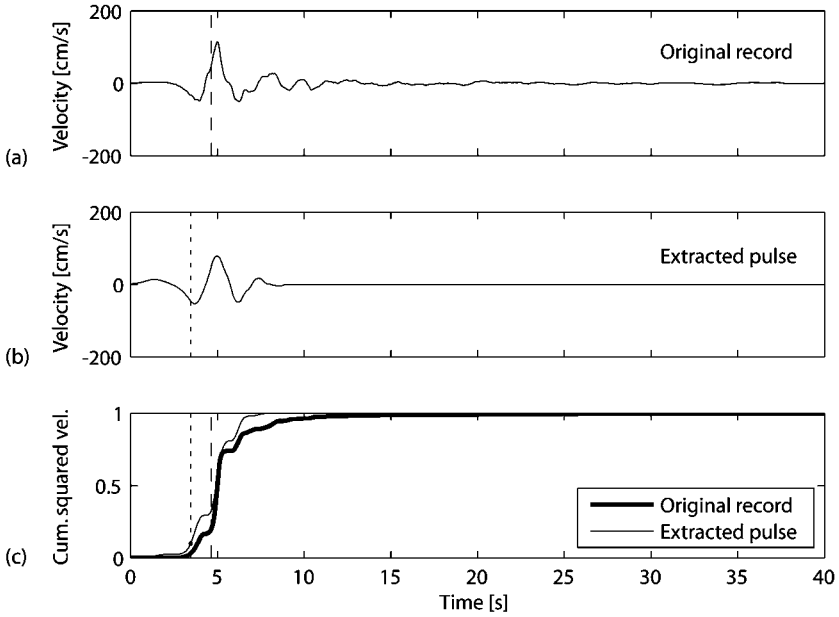

Figure 7. An early-arriving pulse (the 1979 Imperial Valley, EC Meloland Overpass FF recording). (a) Original ground motion. (b) Extracted pulse. (c) Cumulative (Cum.) squared velocities. The times corresponding to $t_{20\%,\text{orig}}$ and $t_{10\%,\text{pulse}}$ are marked with vertical lines.

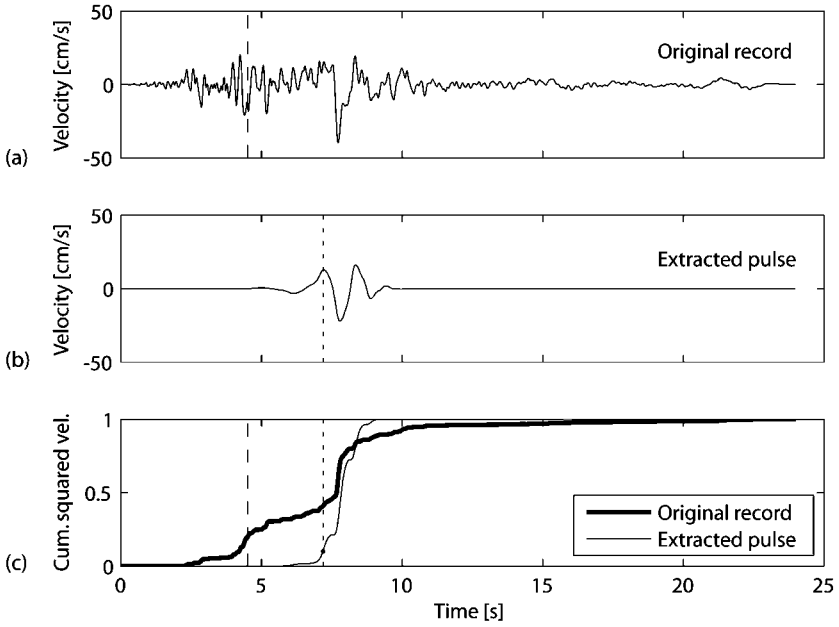

Figure 8. A late-arriving pulse (the 1994 Northridge, Beverly Hills—12520 Mulholland recording). (a) Original ground motion. (b) Extracted pulse. (c) Cumulative (Cum.) squared velocities. The times corresponding to $t_{20\%,\text{orig}}$ and $t_{10\%,\text{pulse}}$ are marked with vertical lines.

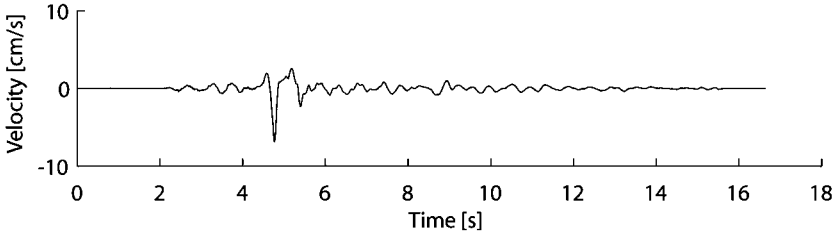

Figure 9. A ground motion that appears to be pulselike, but that could be excluded because of its small PGV value (the LLN recording from a magnitude 5.1 aftershock of the 1983 Coalinga earthquake).

Table 1

Data for All Fault-Normal Ground Motions in the NGA Database That Are Identified as Pulselike Using the Proposed Classification Procedure

No.	Event	Year	Station	T_p	PGV	M_w*	Distance	
							Closest†	Epicentral‡
1	San Fernando	1971	Pacoima Dam (upper left abut)	1.6	116.5	6.6	1.8	11.9
2	Coyote Lake	1979	Gilroy Array #6	1.2	51.5	5.7	3.1	4.4
3	Imperial Valley-06	1979	Aeropuerto Mexicali	2.4	44.3	6.5	0.3	2.5
4	Imperial Valley-06	1979	Agrarias	2.3	54.4	6.5	0.7	2.6
5	Imperial Valley-06	1979	Brawley Airport	4.0	36.1	6.5	10.4	43.2
6	Imperial Valley-06	1979	EC County Center FF	4.5	54.5	6.5	7.3	29.1
7	Imperial Valley-06	1979	EC Meloland Overpass FF	3.3	115.0	6.5	0.1	19.4
8	Imperial Valley-06	1979	El Centro Array #10	4.5	46.9	6.5	6.2	26.3
9	Imperial Valley-06	1979	El Centro Array #11	7.4	41.1	6.5	12.5	29.4
10	Imperial Valley-06	1979	El Centro Array #3	5.2	41.1	6.5	12.9	28.7
11	Imperial Valley-06	1979	El Centro Array #4	4.6	77.9	6.5	7.1	27.1
12	Imperial Valley-06	1979	El Centro Array #5	4.0	91.5	6.5	4.0	27.8
13	Imperial Valley-06	1979	El Centro Array #6	3.8	111.9	6.5	1.4	27.5
14	Imperial Valley-06	1979	El Centro Array #7	4.2	108.8	6.5	0.6	27.6
15	Imperial Valley-06	1979	El Centro Array #8	5.4	48.6	6.5	3.9	28.1
16	Imperial Valley-06	1979	El Centro Differential Array	5.9	59.6	6.5	5.1	27.2
17	Imperial Valley-06	1979	Holtville Post Office	4.8	55.1	6.5	7.7	19.8
18	Mammoth Lakes-06	1980	Long Valley Dam (upper left abut)	1.1	33.1	5.9		14.0
19	Irpinia, Italy-01	1980	Sturno	3.1	41.5	6.9	10.8	30.4
20	Westmorland	1981	Parachute Test Site	3.6	35.8	5.9	16.7	20.5
21	Coalinga-05	1983	Oil City	0.7	41.2	5.8		4.6
22	Coalinga-05	1983	Transmitter Hill	0.9	46.1	5.8		6.0
23	Coalinga-07	1983	Coalinga – 14th & Elm (old CHP)	0.4	36.1	5.2		9.6
24	Morgan Hill	1984	Coyote Lake Dam (southwest abut)	1.0	62.3	6.2	0.5	24.6
25	Morgan Hill	1984	Gilroy Array #6	1.2	35.4	6.2	9.9	36.3
26	Taiwan SMART1(40)	1986	SMART1 C00	1.6	31.2	6.3		68.2
27	Taiwan SMART1(40)	1986	SMART1 M07	1.6	36.1	6.3		67.2
28	N. Palm Springs	1986	North Palm Springs	1.4	73.6	6.1	4.0	10.6
29	San Salvador	1986	Geotech Investigation Center	0.9	62.3	5.8	6.3	7.9
30	Whittier Narrows-01	1987	Downey – company maintenance building	0.8	30.4	6.0	20.8	16.0
31	Whittier Narrows-01	1987	LB – Orange Ave.	1.0	32.9	6.0	24.5	20.7
32	Superstition Hills-02	1987	Parachute Test Site	2.3	106.8	6.5	1.0	16.0
33	Loma Prieta	1989	Alameda Naval Air Station Hanger	2.0	32.2	6.9	71.0	90.8
34	Loma Prieta	1989	Gilroy Array #2	1.7	45.7	6.9	11.1	29.8
35	Loma Prieta	1989	Oakland – Outer Harbor Wharf	1.8	49.2	6.9	74.3	94.0
36	Loma Prieta	1989	Saratoga – Aloha Ave.	4.5	55.6	6.9	8.5	27.2
37	Erzican, Turkey	1992	Erzincan	2.7	95.4	6.7	4.4	9.0
38	Cape Mendocino	1992	Petrolia	3.0	82.1	7.0	8.2	4.5
39	Landers	1992	Barstow	8.9	30.4	7.3	34.9	94.8
40	Landers	1992	Lucerne	5.1	140.3	7.3	2.2	44.0
41	Landers	1992	Yermo Fire Station	7.5	53.2	7.3	23.6	86.0
42	Northridge-01	1994	Jensen Filter Plant	3.5	67.4	6.7	5.4	13.0
43	Northridge-01	1994	Jensen Filter Plant Generator	3.5	67.4	6.7	5.4	13.0
44	Northridge-01	1994	LA – Wadsworth VA Hospital North	2.4	32.4	6.7	23.6	19.6
45	Northridge-01	1994	LA Dam	1.7	77.1	6.7	5.9	11.8
46	Northridge-01	1994	Newhall – West Pico Canyon Rd.	2.4	87.8	6.7	5.5	21.6
47	Northridge-01	1994	Pacoima Dam (downstr)	0.5	50.4	6.7	7.0	20.4
48	Northridge-01	1994	Pacoima Dam (upper left)	0.9	107.1	6.7	7.0	20.4
49	Northridge-01	1994	Rinaldi Receiving Station	1.2	167.2	6.7	6.5	10.9
50	Northridge-01	1994	Sylmar – Converter Station	3.5	130.3	6.7	5.4	13.1
51	Northridge-01	1994	Sylmar – Converter Station East	3.5	116.6	6.7	5.2	13.6
52	Northridge-01	1994	Sylmar – Olive View Med FF	3.1	122.7	6.7	5.3	16.8
53	Kobe, Japan	1995	Takarazuka	1.4	72.6	6.9	0.3	38.6
54	Kobe, Japan	1995	Takatori	1.6	169.6	6.9	1.5	13.1
55	Kocaeli, Turkey	1999	Gebze	5.9	52.0	7.5	10.9	47.0

(*continued*)

Table 1
Continued

No.	Event	Year	Station	T_p	PGV	M_w*	Distance	
							Closest†	Epicentral‡
56	Chi-Chi, Taiwan	1999	CHY006	2.6	64.7	7.6	9.8	40.5
57	Chi-Chi, Taiwan	1999	CHY035	1.4	42.0	7.6	12.7	43.9
58	Chi-Chi, Taiwan	1999	CHY101	4.8	85.4	7.6	10.0	32.0
59	Chi-Chi, Taiwan	1999	TAP003	3.4	33.0	7.6	102.4	151.7
60	Chi-Chi, Taiwan	1999	TCU029	6.4	62.3	7.6	28.1	79.2
61	Chi-Chi, Taiwan	1999	TCU031	6.2	59.9	7.6	30.2	80.1
62	Chi-Chi, Taiwan	1999	TCU034	8.6	42.8	7.6	35.7	87.9
63	Chi-Chi, Taiwan	1999	TCU036	5.4	62.4	7.6	19.8	67.8
64	Chi-Chi, Taiwan	1999	TCU038	7.0	50.9	7.6	25.4	73.1
65	Chi-Chi, Taiwan	1999	TCU040	6.3	53.0	7.6	22.1	69.0
66	Chi-Chi, Taiwan	1999	TCU042	9.1	47.3	7.6	26.3	78.4
67	Chi-Chi, Taiwan	1999	TCU046	8.6	44.0	7.6	16.7	68.9
68	Chi-Chi, Taiwan	1999	TCU049	11.8	44.8	7.6	3.8	38.9
69	Chi-Chi, Taiwan	1999	TCU053	12.9	41.9	7.6	6.0	41.2
70	Chi-Chi, Taiwan	1999	TCU054	10.5	60.9	7.6	5.3	37.6
71	Chi-Chi, Taiwan	1999	TCU056	12.9	43.5	7.6	10.5	39.7
72	Chi-Chi, Taiwan	1999	TCU060	12.0	33.7	7.6	8.5	45.4
73	Chi-Chi, Taiwan	1999	TCU065	5.7	127.7	7.6	0.6	26.7
74	Chi-Chi, Taiwan	1999	TCU068	12.2	191.1	7.6	0.3	47.9
75	Chi-Chi, Taiwan	1999	TCU075	5.1	88.4	7.6	0.9	20.7
76	Chi-Chi, Taiwan	1999	TCU076	4.0	63.7	7.6	2.8	16.0
77	Chi-Chi, Taiwan	1999	TCU082	9.2	56.1	7.6	5.2	36.2
78	Chi-Chi, Taiwan	1999	TCU087	9.0	53.7	7.6	7.0	55.6
79	Chi-Chi, Taiwan	1999	TCU098	7.5	32.7	7.6	47.7	99.7
80	Chi-Chi, Taiwan	1999	TCU101	10.0	68.4	7.6	2.1	45.1
81	Chi-Chi, Taiwan	1999	TCU102	9.7	106.6	7.6	1.5	45.6
82	Chi-Chi, Taiwan	1999	TCU103	8.3	62.2	7.6	6.1	52.4
83	Chi-Chi, Taiwan	1999	TCU104	12.0	31.4	7.6	12.9	49.3
84	Chi-Chi, Taiwan	1999	TCU128	9.0	78.7	7.6	13.2	63.3
85	Chi-Chi, Taiwan	1999	TCU136	10.3	51.8	7.6	8.3	48.8
86	Northwest China-03	1997	Jiashi	1.3	37.0	6.1		19.1
87	Chi-Chi, Taiwan-03	1999	CHY024	3.2	33.1	6.2	19.7	25.5
88	Chi-Chi, Taiwan-03	1999	CHY080	1.4	69.9	6.2	22.4	29.5
89	Chi-Chi, Taiwan-03	1999	TCU076	0.9	59.4	6.2	14.7	20.8
90	Chi-Chi, Taiwan-06	1999	CHY101	2.8	36.3	6.3	36.0	50.0
91	Yountville	2000	Napa Fire Station #3	0.7	43.0	5.0		9.9

*Moment magnitude.
†Closest distance from the recording site to the ruptured area (if available).
‡Distance from the recording site to the epicenter.

period associated with the maximum Fourier amplitude of a wavelet can be used to define a pseudoperiod. To illustrate, an example wavelet and the sine wave with period equal to the wavelet's maximum Fourier amplitude are shown in Figure 10. The pseudoperiod of the largest wavelet coefficient is used here as the ground motion's pulse period. These periods are tabulated in Table 1 for the identified pulselike ground motions. (Note that, with any pulse period measurement approach, the presence and shape of pulses may be affected by filtering of the ground motions at periods near the pulse period. None of the pulse periods reported in Table 1 fall outside the range of usable periods, as determined by low-pass filter frequencies used when processing the ground motions.)

Several other methods have been proposed for determining the period of a velocity pulse. Some methods count zero crossings or use nonlinear optimization to fit a truncated sine wave to the pulse (e.g., Menun and Fu, 2002; Mavroeidis and Papageorgiou, 2003; Bray and Rodríguez-Marek, 2004; Akkar *et al.*, 2005). These methods also provide accurate pulse periods, but have the slight disadvantage of requiring at least a minor degree of user judgment (to judge zero crossings in the presence of noise or to select reasonable starting points so that the optimization converges). Pulse periods obtained from these methods were not reproduced here, but it is expected that they would be very similar to the periods obtained using wavelet analysis.

The primary fully automated alternative for determining

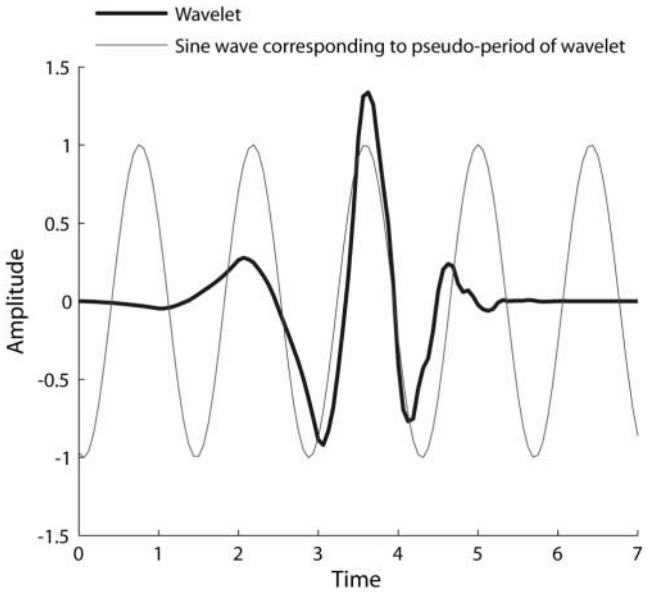

Figure 10. A Daubechies wavelet and a sine wave with period equal to the maximum of the wavelet's Fourier spectrum.

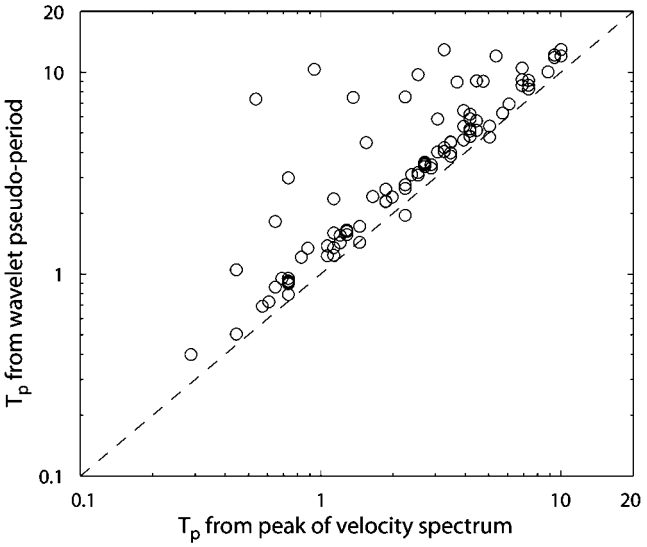

Figure 11. T_p from peak of velocity spectrum versus T_p from the wavelet pseudo-period for the 91 near-fault ground motions.

a pulse period is to select the period associated with the peak of the original ground motion's velocity response spectrum. A plot of pulse-period values from the wavelet and spectral velocity approaches is shown in Figure 11 for the 91 pulse-like ground motions from Table 1. The periods obtained using the two approaches are usually similar, with the wavelet-based T_p being slightly larger, in general, than the spectral-velocity-based T_p. (Note that Bray and Rodríguez-Marek [2004], also observe T_p values slightly larger than spectral-velocity-based T_p when fitting pulse periods in the time domain.)

In cases where the periods obtained from the wavelet and the velocity spectrum methods differ significantly, the wavelet period appears to be the more robust measure of pulse period. In these cases, the period with maximum spectral velocity is associated, in general, with a high-frequency oscillatory portion of the ground motion, whereas the wavelet pulse period is associated with the visible velocity pulse. An example of this is shown in Figure 12. The primary zero crossings associated with this ground motion's pulse are located 7.3 sec apart. The peak spectral velocity of this record occurs at a period of 1.4 sec, whereas the wavelet pseudo-period of 7.5 sec closely matches the period of the pulse identified visually.

Because the wavelet pseudoperiod is identified automatically without a need for user judgment, and because it provides a more consistent identification of the pulse period than the alternative automated method based on the period with peak spectral velocity, this approach appears to be an ideal method for determining the period of velocity pulses in ground motions.

Considering More than One Dimension of Motion

The primary focus in this article is on the fault-normal components of ground motions, but the proposed procedure can also be applied to two-component ground motions. The velocity time history of the Chi-Chi, Taiwan, Tsaotun (TCU075) ground motion is shown in Figure 13. There is a clear velocity pulse in the fault-normal component, and no pulse in the fault-parallel component, as indicated by their pulse indicator scores of 0.999 and 0.001, respectively. By rotating the two-component ground motions, one can compute pulse indicator scores for arbitrary orientations. These pulse scores are shown for the TCU075 ground motion in Figure 14. A pulse is indicated for more than one-half of the range of angles, suggesting that near-fault pulses can affect structures in a variety of directions. This is because the velocity pulse, even when observed at an angle other than its primary direction, can still be large relative to the smaller motions associated with the nonpulse portion of the record. Further, other ground motions indicate that the velocity pulse sometimes occurs at an orientation that differs greatly from the fault-normal orientation. These phenomena have been observed before (Mavroeidis and Papageorgiou, 2002; Howard *et al.*, 2005), and the proposed pulse indicator provides a method to quantify the range of angles for which velocity pulses are of concern. By performing this 3D analysis for a large record set, trends between record orientation and the strength of pulses can be investigated. These results will have useful applications for engineering design situations where the fault orientations of potential future earthquakes are known and it must be determined for which orientations pulselike ground motions may be present.

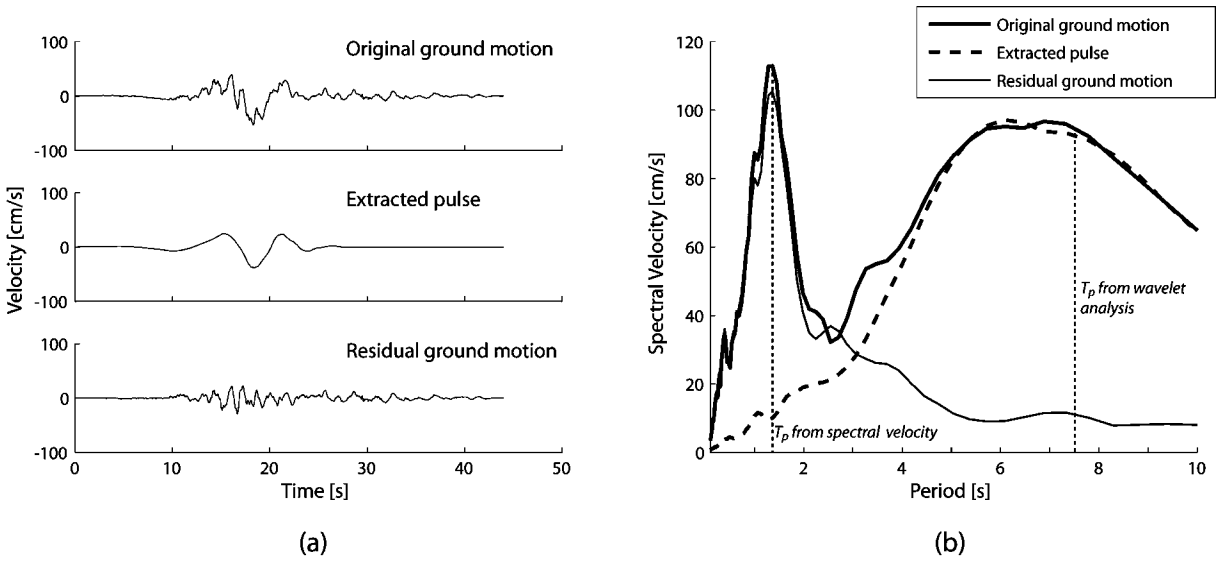

Figure 12. The original ground motion, extracted pulse, and residual ground motion for the 1992 Landers, Yermo Fire Station, ground motion. (a) Velocity time histories. (b) Velocity spectra, with labels noting the T_p values determined using the spectral velocity and wavelet analysis criteria.

Observed Pulses as a Function of Seismological Parameters

The proposed classification criteria do not include seismological parameters such as station location relative to the fault rupture. Theoretical seismology indicates, however, that some station locations are more likely than others to experience near-fault velocity pulses caused by directivity effects (i.e., sites with small source–site distances located such that the fault rupture is propagating toward the site). Because this classification procedure does not depend on those parameters, it presents an opportunity to compare empirical observations with theoretical models for observed directivity effects. To illustrate, the locations of recorded pulselike and non-pulselike ground motions from the 1979 Imperial Valley earthquake are shown in Figure 15. Velocity pulses in general are observed at locations near the fault where the rupture propagates toward the recording station. Note that the late-arriving pulse and PGV $>$ 30 cm/sec criteria do not influence any of the classifications shown in this figure, so the presence of pulses (rather than, e.g., attenuation of PGV with distance from the fault) is the sole source of the classifications shown.

Many individual ground-motion parameters can also be compared with the observed occurrence of velocity pulses. One simple result is shown in Figure 16, where a logistic regression prediction and a windowed average calculation both indicate that the probability of occurrence of a velocity pulse is high for small source–site distances and decreases to nearly zero for distances of greater than 30 km.

A frequently investigated relationship for pulselike ground motions is that between pulse period and earthquake magnitude (Mavroeidis and Papageorgiou, 2003; Somerville 2003; Bray and Rodríguez-Marek, 2004). A plot of magnitude versus pulse period for the ground motions and pulse periods identified here is shown in Figure 17. Using linear regression analysis, the following predictive relationship was obtained

$$E[\ln T_p] = -5.78 + 1.02M. \quad (5)$$

Equation (5) is similar to the equations obtained by other authors. The standard deviation of ln T_p determined from this regression is 0.55; this is smaller than the equivalent result (0.70) obtained when T_p is determined using peak spectral velocity. This suggests that the proposed T_p measure may be more closely correlated with magnitude than the T_p values determined using peaks of velocity spectra.

Iervolino and Cornell (unpublished manuscript, 2007) have performed a more extensive statistical analysis of this type and have also compared pulselike data sets defined by several different authors. Interesting predictor variables include the earthquake's magnitude and distance, the ground-motion orientation relative to the fault, and seismological parameters such as those proposed by Somerville *et al.* (1997) and Spudich *et al.* (2004). The outputs from these predictive relationships are directly applicable for probabilistic seismic hazard analysis and for applications where analysts are trying to select representative ground motions for a site that may experience directivity effects.

Software

The algorithms described are currently implemented in the Matlab programming environment, utilizing the Matlab

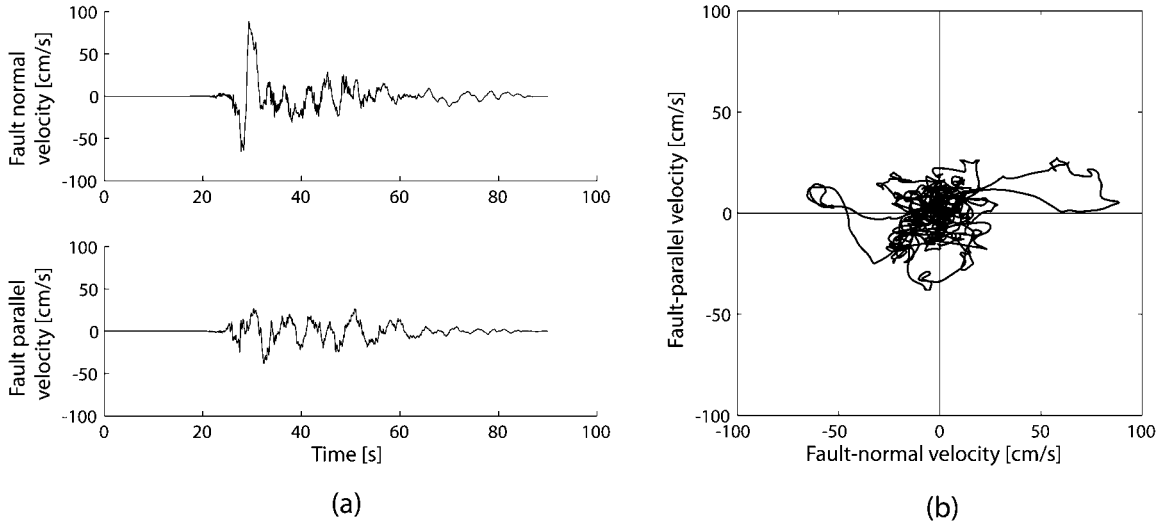

Figure 13. Velocity time history of the Chi-Chi, Taiwan, Tsaotun (TCU075) ground motion. (a) Fault-normal and fault-parallel velocity time histories. (b) Fault-normal versus fault-parallel velocity.

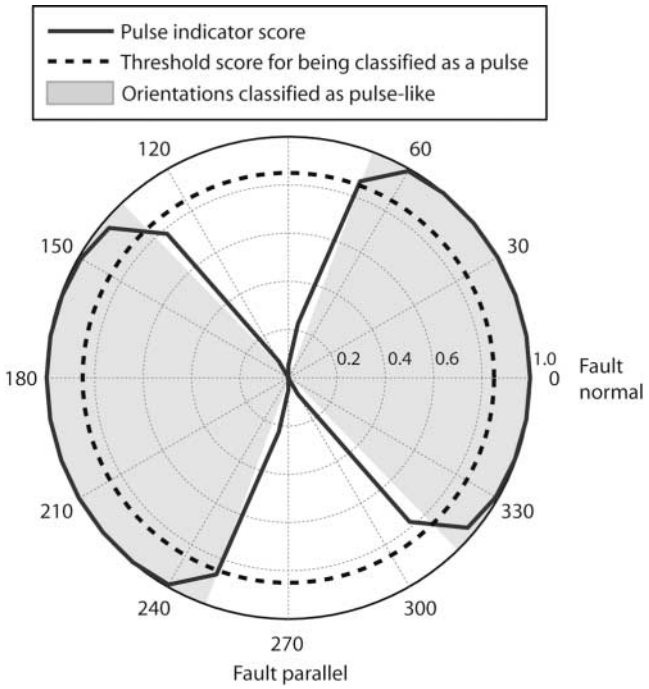

Figure 14. Pulse indicator scores for the Chi-Chi, Taiwan, Tsaotun (TCU075) ground motion as a function of orientation. The angle on the plot indicates the angle of the ground motion relative to fault normal, and the radial magnitude indicates the pulse indicator score from equation (3) for that orientation.

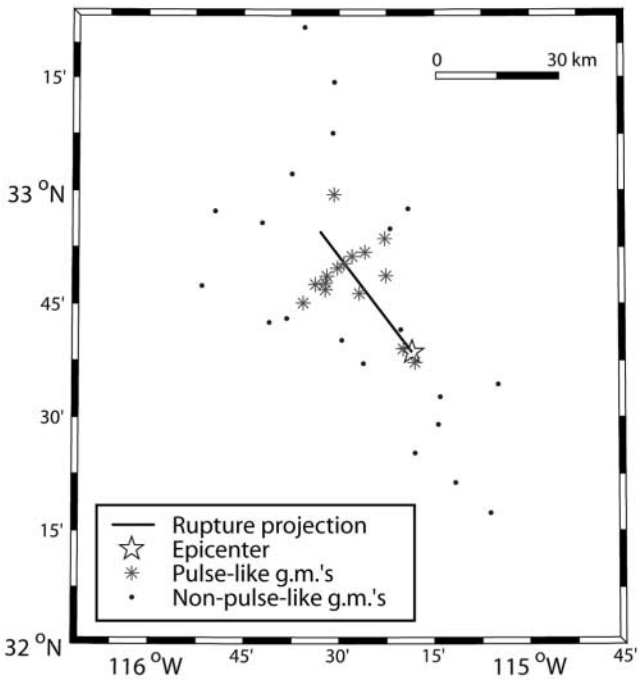

Figure 15. Map view of rupture projection and observed ground motions from the 1979 Imperial Valley earthquake.

Wavelet Toolbox. Source code and associated documentation are available on a dedicated web site at www.stanford.edu/~bakerjw/pulse-classification/. The web site also contains pulse indicator scores, pulse periods, and other relevant information for the entire NGA ground-motion library. The current algorithm requires less than 5 sec on a desktop computer to analyze a ground motion consisting of 5000 data points. A fully open-source implementation of this algorithm is planned to facilitate more widespread adoption of the approach.

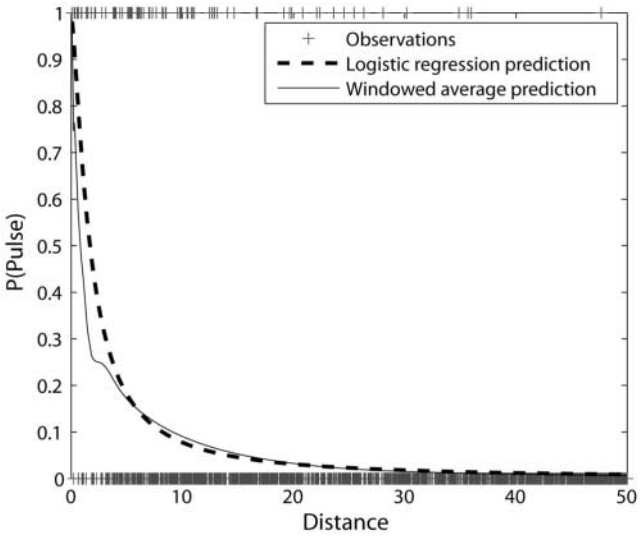

Figure 16. Probability of observing a pulse versus closest distance to fault rupture. Observed pulselike and non-pulselike ground motions are plotted with ordinates of one and zero, respectively.

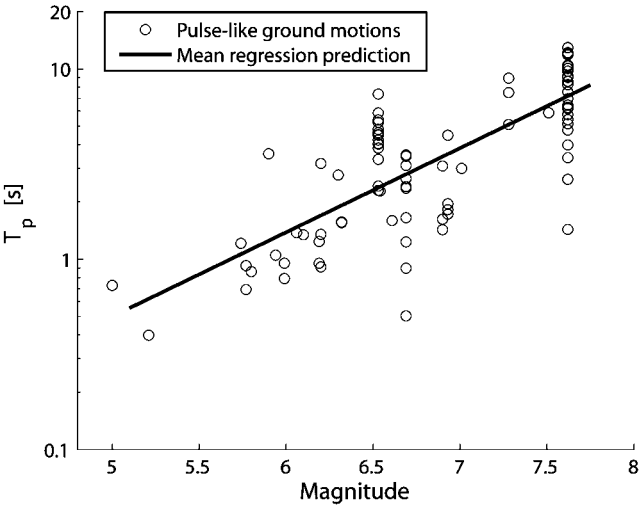

Figure 17. Pulse period versus earthquake magnitude for the pulselike ground motions.

Summary

A procedure has been described for quantitatively identifying velocity pulses in near-fault ground motions. The approach uses the wavelet transform to extract pulselike signals from a ground-motion time history and then classifies the ground motion by comparing the original ground motion with the residual ground motion after the pulse has been extracted. The ratios of PGV and energy between the original and residual ground motions were found to be effective predictor variables for this classification. If pulselike ground motions caused by directivity effects are of primary concern, two additional criteria are proposed to exclude ground motions with pulses arriving late in the record and low-intensity ground motions with simple time histories that coincidentally appear to be pulselike.

The procedure is based purely on signal-processing techniques; the ground motion's source–site geometry is not used when making a classification. This offers an opportunity to compare empirical observations of velocity pulse occurrence with theoretical predictions of directivity-induced pulse occurrence. Alternatively, source–site geometry constraints could be added to the classification approach to identify, for example, pulses resulting from directivity effects. Comparisons of the classifications with other predictor variables indicate that ground motions exhibiting near-fault directivity effects can be identified fairly consistently. Some manual postprocessing may be needed, however, if one wants to ensure that all identified ground motions are, in fact, caused by directivity effects. A table of fault-normal ground motions potentially containing directivity pulses was reported.

Multicomponent ground motions were also considered. By performing the classification at several orientations, it is possible to determine the range of orientations over which a horizontal ground motion appears to be pulselike. Results indicate that directivity effects are observed at a large range of orientations. Statistical analysis of these data obtained from large libraries of ground motions will allow for prediction of pulse occurrence at arbitrary fault orientations rather than only fault-normal and fault-parallel orientations.

The classifications obtained are useful for determining the probability of observing a pulse as a function of earthquake magnitude, distance, source–site geometry, etc. This computation can be obtained using statistical analysis and is a required result for probabilistic seismic hazard analysis that incorporates the possibility of pulse occurrence. Previous collections of pulselike ground motions were not sufficient for computing occurrence probabilities because the ground motions classified as non-pulselike were not reported, so it was not possible to identify the relative fraction of ground motions identified as pulselike.

The procedure is automated and fully quantitative, so classifications can be reproduced exactly by multiple researchers. It is feasible to process thousands of ground-motion time histories in an automated manner with reasonable computational expense, making this a useful tool for parametric studies of pulse occurrence and the relationship between velocity pulses and structural response. The specific criteria used here for classification can modified or supplemented depending on the specific goals of individual scientists and engineers, but the proposed tools and approach should provide a useful foundation for a range of further research activities.

Acknowledgments

Thanks to David Boore, Allin Cornell, David Donoho, Krishnan Kesevan, Iunio Iervolino, and Gee Liek Yeo for providing valuable feedback

during the development of this article. Thanks to Kara Demsey for editing the final manuscript. This work was supported in part by the Earthquake Engineering Research Centers Program of the National Science Foundation, under award number EEC-9701568 through the Pacific Earthquake Engineering Research Center (PEER). Any opinions, findings, and conclusions or recommendations expressed in this material are those of the author and do not necessarily reflect those of the National Science Foundation.

References

Agresti, A. (2002). *Categorical Data Analysis*, Wiley, New York, 710 pp.

Akkar, S., U. Yazgan, and P. Gulkan (2005). Drift estimates in frame buildings subjected to near-fault ground motions, *J. Struct. Eng.* **131,** no. 7, 1014–1024.

Alavi, B., and H. Krawinkler (2001). Effects of near-fault ground motions on frame structures, Blume Center Report 138, Stanford, California, 301 pp.

Anderson, J. C., and V. V. Bertero (1987). Uncertainties in establishing design earthquakes, *J. Struct. Eng.* **113,** no. 8, 1709–1724.

Bertero, V., S. Mahin, and R. Herrera (1978). Aseismic design implications of near-fault San Fernando earthquake records, *Earthquake Eng. Struct. Dyn.* **6,** no. 1, 31–42.

Bray, J. D., and A. Rodríguez-Marek (2004). Characterization of forward-directivity ground motions in the near-fault region, *Soil Dyn. Earthquake Eng.* **24,** no. 11, 815–828.

Fu, Q., and C. Menun (2004). Seismic-environment-based simulation of near-fault ground motions, in *Proc. 13th World Conference on Earthquake Engineering*, Vancouver, Canada, 1–6 August 2004, 15 pp.

Hall, J. F., T. H. Heaton, M. W. Halling, and D. J. Wald (1995). Near-source ground motion and its effects on flexible buildings, *Earthquake Spectra* **11,** no. 4, 569–605.

Howard, J. K., C. A. Tracy, and R. G. Burns (2005). Comparing observed and predicted directivity in near-source ground motion, *Earthquake Spectra* **21,** no. 4, 1063–1092.

Iwan, W. D. (1997). Drift spectrum: measure of demand for earthquake ground motions, *J. Struct. Eng.* **123,** no. 4, 397–404.

Luco, N., and C. A. Cornell (2007). Structure-specific scalar intensity measures for near-source and ordinary earthquake ground motions, *Earthquake Spectra* **23,** no. 2, 357–392.

Makris, N., and C. Black (2003). Dimensional analysis of inelastic structures subjected to near fault ground motions, Earthquake Engineering Research Center, EERC 2003-05, Berkeley, California, 96 pp.

Mallat, S. G. (1999). *A Wavelet Tour of Signal Processing*, Academic Press, San Diego, 637 pp.

Mavroeidis, G. P., and A. S. Papageorgiou (2002). Near-source strong ground motion: characterizations and design issues, in *Proc. 7th U.S. National Conference on Earthquake Engineering*, Boston, Massachusetts, CD-ROM.

Mavroeidis, G. P., and A. S. Papageorgiou (2003). A mathematical representation of near-fault ground motions, *Bull. Seism. Soc. Am.* **93,** no. 3, 1099–1131.

Mavroeidis, G. P., G. Dong, and A. S. Papageorgiou (2004). Near-fault ground motions, and the response of elastic and inelastic single-degree-of-freedom (SDOF) systems, *Earthquake Eng. Struct. Dyn.* **33,** no. 9, 1023–1049.

Menun, C., and Q. Fu (2002). An analytical model for near-fault ground motions and the response of SDOF systems, in *Proc. 7th U.S. National Conference on Earthquake Engineering*, Boston, Massachusetts, 10 pp.

Somerville, P. G. (2003). Magnitude scaling of the near fault rupture directivity pulse, *Phys. Earth Planet. Interiors* **137,** no. 1, 12.

Somerville, P. G., N. F. Smith, R. W. Graves, and N. A. Abrahamson (1997). Modification of empirical strong ground motion attenuation relations to include the amplitude and duration effects of rupture directivity, *Seism. Res. Lett.* **68,** no. 1, 199–222.

Spudich, P., B. S. Chiou, R. W. Graves, K. R. Collins, and P. G. Somerville (2004). A formulation of directivity for earthquake sources using isochrone theory, *U.S. Geol. Surv. Open-File Rept. 2004-1268*, 54 pp.

Tothong, P., C. A. Cornell, and J. W. Baker (2007). Explicit-directivity-pulse inclusion in probabilistic seismic hazard analysis, *Earthquake Spectra* (in press).

Department of Civil and Environmental Engineering
Stanford University
Stanford, California 94305-4020

Manuscript received 8 December 2006.